Optics and Lasers in Engineering 65 (2015) 18–27

Contents lists available at ScienceDirect

Optics and Lasers in Engineering

journal homepage: www.elsevier.com/locate/optlaseng

Digital image correlation in experimental mechanics and image registration in computer vision: Similarities, differences and complements

Zhaoyang Wang [a,*], Hien Kieu [b], Hieu Nguyen [b], Minh Le [b]

[a] Department of Mechanical Engineering, The Catholic University of America, Washington, DC 20064, USA
[b] Department of Electrical Engineering and Computer Science, The Catholic University of America, Washington, DC 20064, USA

ARTICLE INFO

Article history:
Received 27 February 2014
Received in revised form
6 April 2014
Accepted 6 April 2014
Available online 24 April 2014

Keywords:
Digital image correlation
Image registration
Image matching
Experimental mechanics
Computer vision

ABSTRACT

Digital image correlation and image registration or matching are among the most widely used techniques in the fields of experimental mechanics and computer vision, respectively. Despite their applications in separate fields, both techniques primarily involve detecting the same physical points in two or more images. In this paper, a brief technical comparison of the two techniques is reviewed, and their similarities and differences as well as complements are presented. It is shown that some concepts from the image registration or matching technique can be applied to the digital image correlation technique to substantially enhance its performance, which can help broaden the applications of digital image correlation in scientific research and engineering practice.

1. Introduction

Digital image correlation (DIC) and image registration or matching (hereinafter referred to as "IRM") are currently among the most widely used techniques in the fields of experimental mechanics and computer vision, respectively. Their popularity and prevalence originate from the rapid evolution of computer and imaging technology. The DIC technique has been used in the mechanics and optics fields for deformation, shape and motion measurements, whereas the IRM technique has become an essential process in computer vision for numerous applications in a variety of fields. Despite that the DIC and IRM techniques are being used in different applications, both techniques mainly involve detecting the same physical points in two or multiple images. In this paper, a brief comparison of the two techniques is presented, and their complements are described. The goal is to introduce some valuable achievements in computer vision to experimental mechanics.

1.1. History

An investigation of the history of the DIC and IRM techniques will not be complete without looking at the history of photogrammetry [1], which can be dated back to Leonardo da Vinci's work in 1400s. Nevertheless, the ground-laying work of both the DIC and IRM techniques that led to their current prosperity seems happened in the very early 1980s.

In the field of experimental mechanics, it is believed that Peters and Ranson first proposed to use a DIC-like method to conduct deformation measurement in 1982 [2]. Then Sutton and colleagues improved the original concept and made the DIC technique practically suitable for surface deformation measurements in a variety of applications [3–7]. After that, the 1990s and the first few years of the 21st century had seen a steady and limited growth on the studies and applications of the DIC technique, which was sometimes given other names. Since 2005, the DIC technique has undergone a tremendous growth worldwide [8,9]. A notable evidence is that many of the aforementioned papers have been each cited a few hundreds of times.

In the field of computer vision, there were many studies on the IRM technique before 1980s [10], yet the classic work was published by Lucas and Kanade in 1981 [11]. Numerous algorithms and a wide variety of their extensions were later proposed to enhance the original formulation. Particularly, an algorithm-unifying study was conducted in 2001 and the related work involving an inverse-compositional algorithm was published in detail in 2004 [12]. The inverse-compositional algorithm is equivalent to the standard forwards-additive algorithm commonly used by the DIC technique, but it is technically more efficient [9,13]. For this reason, many DIC

* Corresponding author.
E-mail addresses: wangz@cua.edu, wzyly@yahoo.com (Z. Wang).

http://dx.doi.org/10.1016/j.optlaseng.2014.04.002
0143-8166/

codes have adopted the inverse-compositional approach since then. In the meanwhile, an evaluation tool has been available for algorithm assessment [14,15] and there have been numerous advances achieved in the IRM technique, which motivated this paper for a brief comparison of the DIC and IRM techniques.

1.2. Journals and conferences

The mechanics and computer vision communities nearly have no dialog between them. Therefore, it is helpful to list a number of representative journals and conferences that frequently cover the DIC and IRM techniques in each field.

- DIC: Experimental mechanics, Strain, Journal of strain analysis for engineering design, Optics and lasers in engineering, Optics and lasers technology, Optics letters, Optics express, Applied optics, Optical engineering, Measurement and science technology, Society for experimental mechanics (SEM) annual conference and exposition on experimental and applied mechanics, International conference on experimental mechanics (ICEM), etc.
- IRM: IEEE transactions on pattern analysis and machine intelligence, International journal of computer vision, IEEE transactions on image processing, Pattern recognition, Image and vision computing, Journal of mathematical imaging and vision, Computer vision and image understanding, Medical image analysis, IEEE conference on computer vision and pattern recognition (CVPR), IEEE international conference on computer vision (ICCV), European conference on computer vision (ECCV), etc.

2. Similarities

2.1. Image matching

The fundamental work of both the DIC and IRM techniques is to geometrically align two images (named reference and target images) by detecting the same physical points in these two images that are captured from different viewpoints, at different time, and/or by different cameras. The DIC technique generally uses area-based (also known as intensity-based) matching, and the IRM technique uses both area-based and feature-based matching. The common area-based matching scheme is described below.

The area-based matching employs a correlation criterion to detect the best matching for a group of pixels (named subset) centered at each feature pixel to be interrogated. There exist a variety of correlation criteria, and a simple yet robust criterion named the parametric sum of squared difference criterion can be written as [16]:

$$C=\sum_{i=1}^{N}[af(x_i,y_i)+b-g(x_i',y_i')]^2 \tag{1}$$

where a is a scale factor, b is an offset of intensity, and $f(x_i,y_i)$ and $g(x_i',y_i')$ indicate the intensity values at the ith pixel in the reference subset and the matching pixel in the target subset, respectively. The task of the correlation analysis is to minimize the coefficient C in Eq. (1) to detect the best matching. For a typical pixel (x_0,y_0) to be analyzed in the reference image, a square pattern of $N=(2M+1)\times(2M+1)$ pixels with its center located at (x_0,y_0) is usually chosen as the reference subset. The corresponding subset in the target image, i.e., the target subset, is often of irregular shape. Denoting the translation amount between the centers of the two matching subset patterns as (ξ,η), a shape mapping function for the entire reference and target subsets can be expressed as

$$x_i'=x_i+\xi+\xi_x\Delta_x+\xi_y\Delta_y+\xi_{xx}\Delta_x^2+\xi_{yy}\Delta_y^2+\xi_{xy}\Delta_x\Delta_y$$

$$y_i'=y_i+\eta+\eta_x\Delta_x+\eta_y\Delta_y+\eta_{xx}\Delta_x^2+\eta_{yy}\Delta_y^2+\eta_{xy}\Delta_x\Delta_y \tag{2}$$

where $i=1,2,\ldots,N$; $\Delta_x=x_i-x_0$; $\Delta_y=y_i-y_0$; ξ_x, ξ_y, ξ_{xx}, ξ_{yy}, ξ_{xy}, η_x, η_y, η_{xx}, η_{yy}, and η_{xy} are the coefficients of the shape function. To determine all the 12 unknowns of the shape function (ξ, η, and the above 10 coefficients) as well as the scale and offset parameters (a and b) involved in Eq. (1), the matching technique often employs an iterative algorithm such as the Levenberg–Marquardt method to carry out the correlation optimization. The iterative algorithm is capable of providing very fast and highly accurate correlation analysis [17] upon a reasonably good initial guess for the unknowns (mainly the lower order terms ξ, η, ξ_x, ξ_y, η_x, η_y). Such an initial guess can be traditionally detected by an automated scanning process for simple cases [18,19] or a manual human–computer interaction way for complex cases.

2.2. Camera calibration

Camera calibration is technically not a part of the DIC and IRM techniques. In practice, however, camera calibration is often essential to the enormous applications of the DIC and IRM techniques.

Camera calibration has been a very active research topic in the last two decades, and numerous advances have been made since the work of Tsai [20]. The most successful model, the pinhole model, for camera calibration describes the relation between the 3D world coordinate of a calibration target point $\boldsymbol{M}=[X_w,Y_w,Z_w]^T$ and its corresponding location $\boldsymbol{m}=[u,v]^T$ in the image plane as

$$\lambda\begin{bmatrix}\boldsymbol{m}\\1\end{bmatrix}=\begin{bmatrix}\alpha&\gamma&u_0\\0&\beta&v_0\\0&0&1\end{bmatrix}\begin{bmatrix}R_{11}&R_{12}&R_{13}&T_1\\R_{21}&R_{22}&R_{23}&T_2\\R_{31}&R_{32}&R_{33}&T_3\end{bmatrix}\begin{bmatrix}\boldsymbol{M}\\1\end{bmatrix} \tag{3}$$

where λ is a scale factor, α and β are the horizontal and vertical focal lengths in pixel unit, γ is a skew factor, and (u_0,v_0) is the coordinates of the principal point, $\boldsymbol{R}$ and $\boldsymbol{T}$ are the extrinsic parameters that denote the rotation and translation relating the world coordinate system to the camera coordinate system, respectively. Because of the nonlinear optical distortion, a lens distortion model is also necessary for an accurate camera calibration. Currently, a general lens distortion model is expressed as

$$\begin{aligned}u'&=(1+a_0r^2+a_1r^4+a_2r^6+a_3r^8+a_4r^{10})u\\&\quad+(s_0+s_2r^2)r^2+(p_0+p_2r^2)(r^2+2u^2)\\v'&=(1+a_0r^2+a_1r^4+a_2r^6+a_3r^8+a_4r^{10})v\\&\quad+(s_1+s_3r^2)r^2+(p_1+p_3r^2)(r^2+2v^2)\\r^2&=u^2+v^2\end{aligned} \tag{4}$$

where (a_0,a_1,a_2,a_3,a_4), (s_0,s_1,s_2,s_3), and (p_0,p_1,p_2,p_3) represent the radial, prism, and tangential distortion coefficients, respectively; (u,v) denotes the distortion-free pixel location, and (u',v') is the corresponding distorted point. To avoid calculation instability during the calibration process, (u,v) and (u',v') in the equation are usually converted to their normalized terms.

Given the locations of the calibration control points in the world coordinate as $\boldsymbol{M}_i$ and in the image plane as $\boldsymbol{m}_{ij}$, the calibration process involves a nonlinear optimization with the cost function defined as

$$S=\sum_{i=1}^{i=k}\sum_{j=1}^{j=l}\|\boldsymbol{m}_{ij}-P(\boldsymbol{A},\boldsymbol{\varphi},\boldsymbol{r},\boldsymbol{T},\boldsymbol{M}_i)\|^2 \tag{5}$$

where k and l denote the number of control points and the number of images, respectively; $\boldsymbol{A}$ indicates the intrinsic camera parameters $(\alpha,\beta,\gamma,u_0,v_0)$ as shown in Eq. (3); $\boldsymbol{\varphi}$ represents all the lens distortion parameters $(a_0,\ldots,p_3)$; P denotes the projection of control points onto the image planes according to Eqs. (3) and (4); $\boldsymbol{r}$ is the Rodrigues vector of the rotation matrix $\boldsymbol{R}$; and $\boldsymbol{T}$ is the translation vector.

Zhang introduced the original impressive algorithm that requires only a few images of a planar checker board to compute the camera parameters [21]. The approach consists of an initial closed form solution of the camera parameters, followed by Levenberg–Marquardt nonlinear refinement of Eq. (5). Each work of Tsai and Zhang has been cited a few thousand times in the literature and they have inspired the well-known OpenCV and MATLAB camera calibration packages, which allow a regular camera to achieve an accuracy around 0.1 pixels in terms of the reprojection root-mean-squared-error (RMSE) using paper-printed checker patterns. On the other hand, by adopting circular control points as an alternative to square patterns and using first order elliptic approximation to take into account the perspective effect, the camera calibration results with RMSE around 0.05 pixels can be achieved in real experiments with the bundle adjustment approach [22–29]. The calibration RMSE can be further reduced to below 0.01 pixels with a frontal image concept [30,31]. It is interesting to note that the frontal image concept actually relies on an area-based template matching algorithm previously described.

With the above approach, the total number of unknowns in camera calibration is $(18+3k+6l-7)$, where "18" comes from the intrinsic parameters in $\boldsymbol{A}$ and $\boldsymbol{\varphi}$, "$3k$" is due to the 3D Cartesian coordinates of k control points $\boldsymbol{M}$, "$6l$" comes from $\boldsymbol{r}$ and $\boldsymbol{T}$ of l board positions, and "-7" is associated with the plane constraints from three arbitrary noncollinear points. Because the world coordinate system can be established on the plane constraints, the camera calibration only requires that the physical distance between any arbitrary two points to be known to determine the physical exact scale. Fig. 1 shows an example of large calibration board with coded circular patterns.

For the calibration of a system with $n(n \geq 2)$ cameras, each additional camera can be added to the calibration model with 18 intrinsic parameters and 6 position parameters with respect to its preceding camera. Thus the total number of unknowns for multi-cameras calibration is $(18n+3k+6l+6[n-1]-7)=(24n+3k+6l-13)$. As mentioned previously, these unknowns can be determined from a nonlinear optimization with the Levenberg–Marquardt algorithm.

3. Differences

Although the DIC and IRM techniques involve the same geometrical work of matching points in one image with the corresponding points in another image, there are a number of differences between them. These differences are due to the nature of their applications in experimental mechanics and computer vision.

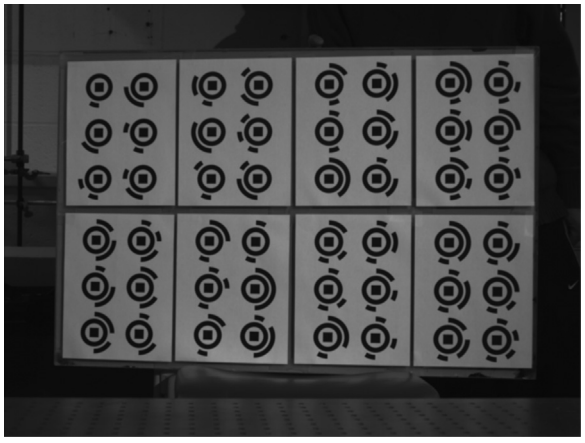

Fig. 1. A large calibration board with coded circular patterns.

3.1. Pattern: artificial vs. natural

Both the DIC and IRM techniques rely on that there are sufficient intensity variations in the reference and target images to ensure reliable point identification and matching. This requires the objects of interest to be covered with natural or artificial texture patterns; ideally, the preferred surface texture patterns should be random and not periodic.

Experimental mechanics applications usually involve specific objects or specimens, and the measurements are often well controlled. To achieve an easy and accurate DIC analysis, the object surfaces are desired to have artificial speckle patterns. In practice, such patterns can be prepared by applying a thin layer of white spray paint on the object surface, followed by an overspray of black paint to obtain random speckle patterns. If the object would have deformation or shape change, strong bonding between the coating and the object is required. In the case of shape measurement only, the speckle patterns can be provided by projecting patterns using a computer and a digital projector.

Unlike the DIC technique, the IRM technique in computer vision applications usually performs feature detection and image matching using the natural patterns occurred in the scenes and on the object surfaces. This can solve the cost and time-consuming issues in artificial pattern fabrication; in the meanwhile, it brings a few challenging problems as follows: (1) The objects or scenes may not have sufficient pattern or texture variations for a reliable matching process, such as matching the points of a uniform white wall. Downsampling the images can help cope with this issue, but the matching accuracy can meanwhile be attenuated. Using the aforementioned artificial projection patterns can also be employed, but the application limitations will arise. (2) The area-based matching scheme can face difficulties if there are multiple objects with substantially different pattern characteristics. This will need a self-adaptive subset selection and an additional handling such as the feature-based matching. However, the advanced special schemes may not be able to always provide reliable matching results [32]. Fig. 2 shows an example of the speckle patterns for the DIC analysis and natural patterns [15] for the IRM processing.

It should be pointed out that because the gray-scale intensity distribution characteristics of the texture patterns can vary a lot in different applications, the accuracy of the final image matching can also vary substantially, as demonstrated in the work of Lecompte et al. [33].

3.2. Matching: area-based matching vs. feature-based matching

Image matching algorithms can be classified into area-based matching and feature-based matching. Because experimental mechanics applications often handle continuous bodies of objects, the area-based algorithm together with artificial patterns is always used in the DIC technique for reliable and accurate matching. For the IRM technique in computer vision, however, because natural patterns and multiple separate objects as well as occlusions and shadows are usually encountered, feature-based algorithms have become essential in many IRM applications.

Feature-based matching algorithms extract features of interest from the images, such as edges or contours, and match them in different images. The matching is fast because only a relatively small number of image pixels are detected as features. The shortcoming is that the matching may fail with incorrect matching and the matched points are very sparsely located. Nevertheless, feature-based matching algorithms have found numerous applications such as object recognition and identification, robotic mapping and navigation, image stitching, gesture recognition, and motion tracking.

The most well-known feature-based matching techniques are the scale-invariant feature transform (SIFT) algorithm [34] and

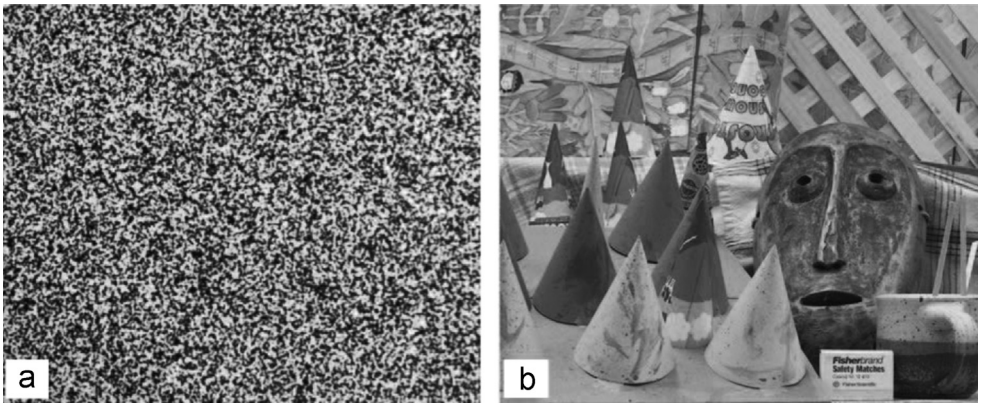

Fig. 2. Examples of natural and artificial texture patterns. (a) Speckle patterns for DIC, (b) natural patterns for IRM.

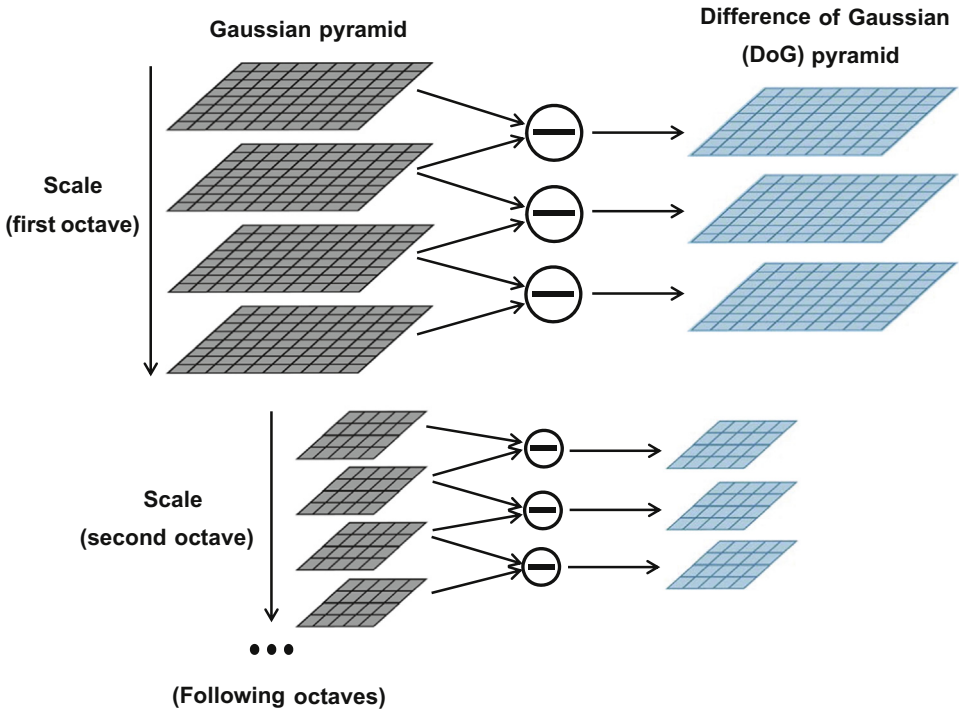

Fig. 3. Scale-space pyramid for SIFT. The image is subsampled by two in every octave.

its extensions such as speeded-up robust features (SURF) algorithm [35] and principal components analysis SIFT (PCA-SIFT) algorithm [36].

The SIFT algorithm aims to extract local features in the images and describes each feature point with a 128-dimensional descriptor. To achieve scale invariance for the feature points, the points are obtained from scale-space extrema of the difference of Gaussian (DoG). This is done by constructing an image pyramid: first, the Gaussian pyramid is formed from the original image by successive smoothing and subsampling. Second, the DoG pyramid is built from the differences of the subsampled images and its Gaussian smoothing version at that pyramid level, as illustrated in Fig. 3. Third, the extrema of the scale-space function are detected by comparing each pixel in the pyramid image with its 26 neighbor pixels. Last, a quadratic polynomial is fitted to the local sample points of each detected extremum to localize it with a higher accuracy.

After the detection of SIFT feature points, the SIFT descriptor uses local intensity-gradient information to summarize the image appearance in a local neighborhood around each feature point. To achieve rotational invariance, each point is assigned an orientation corresponding to the dominant direction computed from a local histogram of gradient directions accumulated over a neighborhood of the point. Before being added to the histogram, each sample's gradient magnitude is weighted by a Gaussian window centered at the interrogated point with the size proportional to its detection scale. After that, a $4\times$ 4 square grid of size proportional to the detection scale of the feature point is laid out in the image, as demonstrated in Fig. 4. An 8-bin accumulated histogram is then generated from the image gradient directions within each grid. This leads to an image SIFT descriptor of $4\times4\times8=128$ dimensions for each feature point. The 128-dimensional histogram is also normalized to unit sum to improve the robustness of the descriptor to illumination invariance.

After the SIFT processing, the matching of feature points between two images can be detected by mutually matching their descriptors and choosing the one that minimizes the Euclidean distance between them. This can be conducted by using a fast library for the approximate nearest neighbors (FLANN) algorithm [37]. Fig. 5 illustrates an example of the SIFT matching result, where a number of matching pairs are detected from two images containing objects placed in various positions.

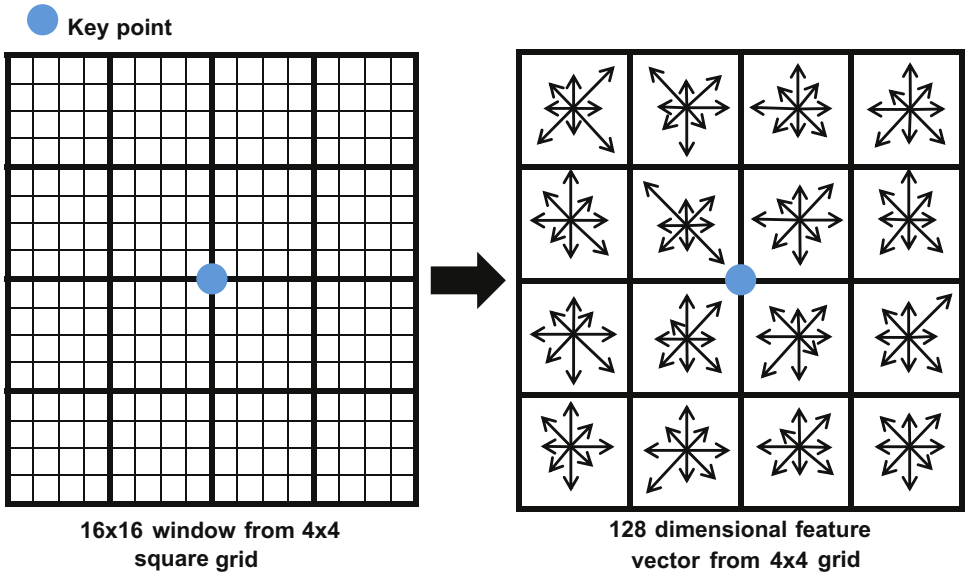

Fig. 4. SIFT descriptor contains 4 × 4 descriptor array calculated from 16 × 16 samples.

Fig. 5. SIFT matching result of a few objects placed in various positions. (a), (b) Two images and (c) the detected FLANN correspondences.

Because there usually exist some false matching points in the SIFT–FLANN matching results, a random sample consensus (RANSAC) algorithm [38] with certain predefined model functions can be utilized to remove those mismatches. Some extensions to the original RANSAC algorithm have been developed in recent years such as PROSAC [39] and GroupSAC [40], and improved RANSAC (iRANSAC) [41] algorithms.

It is noted that the SURF and PCA-SIFT algorithms are developed based on the SIFT algorithm. In general, SIFT slightly outperforms SURF, but SURF provides faster analysis than SIFT by approximating the Laplacian of Gaussian with box filters and using the sums of Haar wavelet responses to assess feature orientations as well as making an efficient use of integral images. Compared with SIFT and SURF, PCA-SIFT can cope better with rotation and illumination changes through applying principal components analysis to the normalized gradient patch instead of using SIFT's smoothed weighted histograms. In addition to SIFT, SURF, and PCA-SIFT, there are a few other notable feature detection algorithms such as smallest univalue segment assimilating nucleus (SUSAN) [42] and features from accelerated segment test (FAST) [43] algorithms, these are however less popular.

3.3. *Speed and accuracy: high vs. low*

With high performance central processing unit (CPU) and graphics processing unit (GPU), both the DIC and IRM processing can be implemented in a real-time manner. In addition, high-speed digital cameras can be employed to satisfy the fast- and high-speed

measurement demands in various experimental mechanics and computer vision applications. Despite that, it is practically useful to examine the typical processing speed of the DIC and IRM techniques. Like many other techniques, there is generally a tradeoff between achieving high speed and high accuracy.

In conventional DIC analysis, a region of interest (ROI) is often specified first in the reference image. Then, the Levenberg–Marquardt optimization process is initiated at the seed point and subsequent computation is conducted at each grid point along each row or column. The computation at each grid point normally needs a few iterations and accurate image interpolation is performed in each iteration. To increase the computation speed while maintaining high analysis accuracy, the family of B-spline interpolation with digital filter scheme and recurrence approach can be used [17]. Many computer simulations have shown that the DIC algorithm can easily yield accuracy better than 0.001 pixels at a speed faster than 5000 points per second. Overall, however, the entire DIC analysis is relatively slow, especially when advanced schemes such as reliability-guided correlation scanning strategy [44] to improve analysis reliability are adopted. It is noteworthy that the DIC technique may use the Fourier domain correlation scheme to speed up the processing; however, this method cannot handle well with the case of large rotation and/or deformation.

In computer vision applications, real-time and fast-speed analysis is often necessary for the IRM technique. Consequently, the feature-based IRM plays a key role in applications such as robotic navigation, gesture recognition, and motion tracking. The fast computation speed is often due to the simple algorithms and matching detection at sparse data locations. Because interpolation is usually applied to get full-field image matching, the matching accuracy is normally low and matching results can be wrongly obtained at unmatchable regions.

In recent years, the establishment of the Middlebury stereo vision evaluation dataset has inspired numerous advances in the IRM algorithms [15]. These algorithms usually work with rectified images and use a non-iterative method to simplify the image matching, and special handling is then employed to tackle discontinuities. At present, the top ranking IRM algorithms can yield reasonable good accuracy to the 2001 and 2003 dataset [15,45–49], but the problem is that they all face difficulties for general real-world problems. Applications of the DIC algorithm to the Middlebury dataset have also been reported [50], but the full-field accuracy is relatively low because the scenes in the dataset are not suitable for the area-based matching used by the DIC algorithm.

4. Complements

The DIC and IRM techniques have been used individually in experimental mechanics and computer vision fields, respectively. Because of the different purposes of application, they put emphasis on different technical aspects. In general, the DIC technique is used in experimental mechanics applications where accuracy is among the most important requirements, whereas the IRM technique is used in computer vision applications where convenience and speed are more demanded. Their similarities and differences imply that there can be complements between each other. For instance, the popular Kinect for Microsoft XBox 360 uses projected infrared texture patterns to reliably acquired depth information in real-time. In this paper, how the DIC technique can learn from the IRM technique is of great interest.

4.1. *Pattern: natural pattern for DIC*

As previously described, the DIC technique requires the object of interest to have speckle or texture patterns on its surface. The speckle patterns are usually artificially prepared by using spray paint, which is a notable limitation of the conventional DIC measurement. Since the IRM technique normally uses natural patterns, it is feasible that the DIC measurement may use natural patterns as well, particularly considering that the 3D-DIC technique for broad applications beyond mechanics field has become an emerging tool.

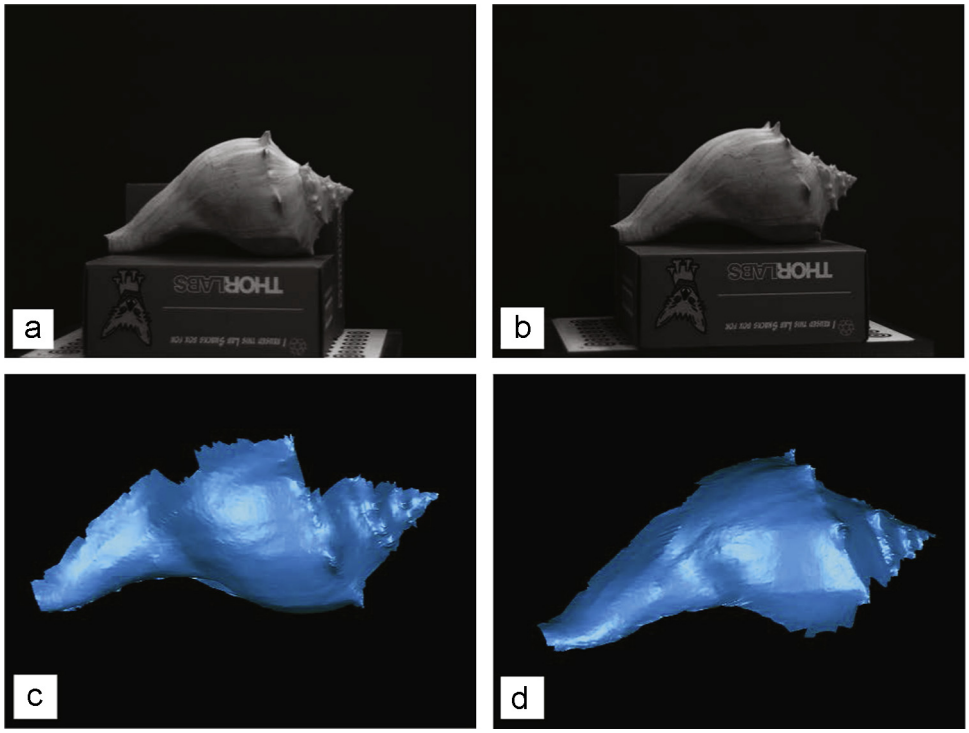

Fig. 6. 3D shape measurement of a conch shell with the 3D-DIC technique. (a), (b) The captured images and (c), (d) two representative 3D plots. Only the shell is analyzed in the measurement.

In the last decade, it has been reported that natural patterns can be used for the DIC technique, but most of them are related to measurements at microscopic scales. For example, Zhang et al. proposed in 2006 that although surface preparation is generally required for displacement measurements using the DIC technique, the natural surface texture of an aluminum specimen is suitable for microscopic measurements if proper illumination is used [51]. A few other work where the natural surface patterns of microstructures were utilized to determine the deformation field at microscopic scales have also been reported [52,53]. In a recent paper, the natural annulus brosus pattern is used to investigate the transverse behavior of annulus tissue samples subjected to uniaxial tensile tests [54]. Actually, early notice about the possibility of using natural pattern for casual DIC measurement is that Marcellier et al. suggested that skin may be naturally featured enough to have a random pattern of its own [55]. However, it is not until Kieu et al. recently showed that the DIC technique can be applied to measure a wide range of different objects with high accuracy [56].

Fig. 6 shows an experimental result of the 3D-DIC shape measurement of a conch shell, where the natural patterns on the shell surfaces provide the required intensity variations. Fig. 7 is another example showing the 3D face measurement of one of the authors, where the skin pores serve as the natural texture patterns.

4.2. Matching: feature-based algorithm for DIC

A noteworthy limitation of the DIC technique is that it needs a good initial guess for the seed or starting point to conduct Levenberg–Marquardt optimization. To overcome this shortcoming, the feature-based matching scheme from the IRM algorithm can be incorporated into the DIC analysis to find matches at sparse point locations, which can serve as initial guess purpose for the DIC analysis regardless of large rotation, deformation, or scale changes. Recently, the SIFT algorithm has been reported by researchers to carry out automated initial guess for the DIC measurement [41,57]. Because the SIFT algorithm can cope well with image scale change, rotation change, lighting change, partial perspective view change, and partial occlusion, it can help provide robust and accurate matches at feature points for automatic initial guess in the DIC measurements in the case of large deformation and rotation as well as periodic texture patterns [41].

Another important limitation of the general DIC analysis is that it cannot propagate through discontinuous regions such as occlusions, shadows or regions that do not have enough intensity variations. This discontinuity problem can be resolved by using the SIFT algorithm as well in the DIC analysis. As proposed in Kieu's paper [56], the SIFT algorithm can be applied to automatically set many seed points in the images and the DIC process can be initiated from each seed point to propagate the analysis until it reaches unmatchable regions like shadows, occlusions, or homogeneous regions which lack sufficient intensity variations for image correlation. By doing this way, the DIC analysis can reach all the matchable regions without any difficulty caused by the discontinuities.

Fig. 8 shows an example of 3D imaging of a few objects with the 3D-DIC technique. The natural patterns on the objects provide the required intensity variations for image matching, and the SIFT algorithm has been employed to automatically cope with the discontinuities.

4.3. Performance: self-adaptive subset and high-speed analysis for DIC

The DIC subset must have an appropriate size and must contain sufficient intensity variations to ensure that they can be uniquely and accurately identified in the images. It can be easily understood that the errors of matching are closely related to the subset sizes for the given images [58–65]. Instead of choosing a fixed subset size like the traditional DIC analysis does, a new DIC approach can borrow an idea from many IRM techniques in computer vision

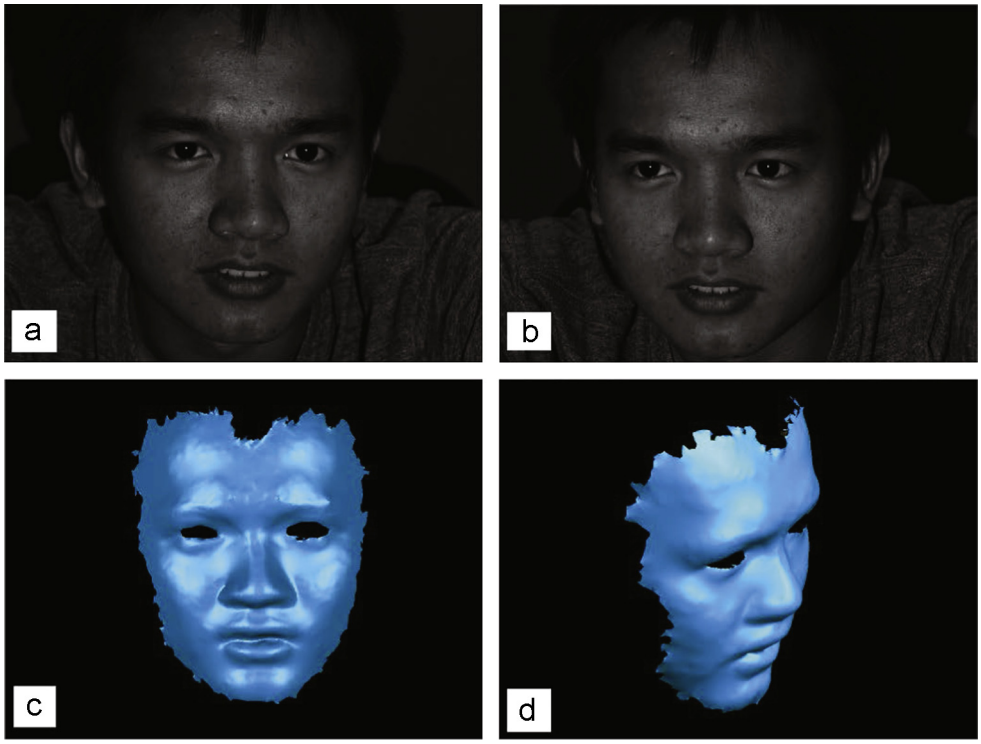

Fig. 7. 3D face profile reconstruction with the 3D-DIC technique. (a), (b) The captured images and (c), (d) two representative 3D plots. Only the face is analyzed in the measurement.

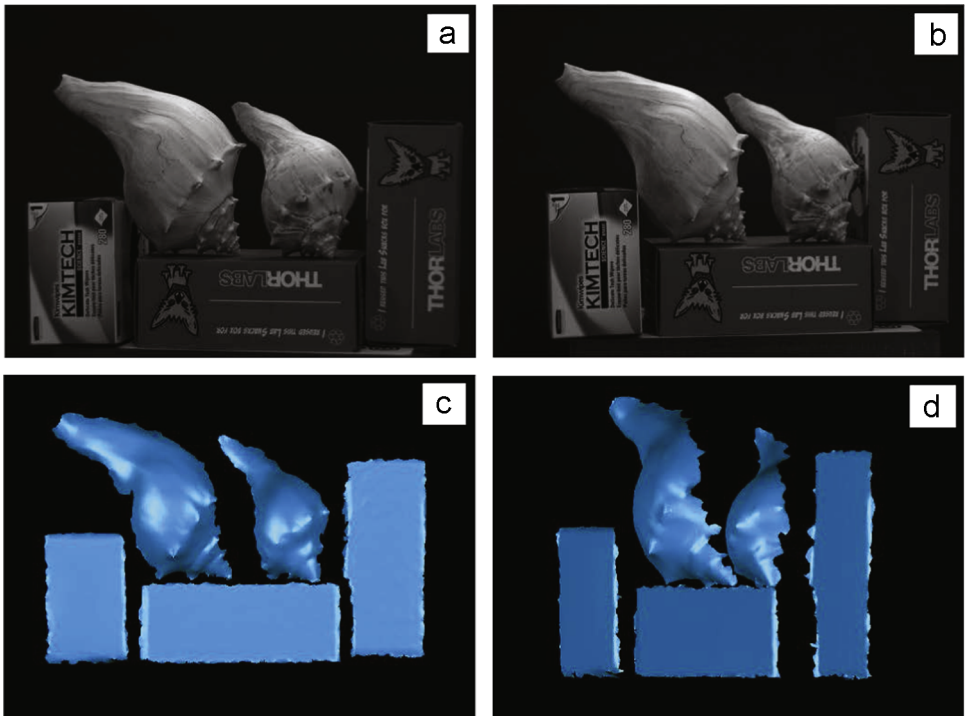

Fig. 8. 3D imaging of a few objects. (a), (b) The captured images and (c), (d) two representative 3D plots.

field by having a flexible subset size based on the pattern features and the scale size of the object to be measured. From the most successful feature-based SIFT technique [34], the DIC process can learn from the SIFT algorithm which matches feature points based on the intensity of a region whose size is determined by the scale at that point. By using a self-adaptive subset that is corresponding to the size of the SIFT feature matching window, the DIC analysis can establish a faster calculation with enhanced accuracy. This is practically very useful in broad DIC applications because the images captured can contain different objects with different scales and features. With a fixed and identical subset size for the entire DIC analysis, it cannot give high analysis accuracy for all the regions and objects.

In addition to scale, the DIC technique can also learn from the SIFT and its extension algorithms in which rotation variance can be handled very well. The window for calculating the descriptor of the SIFT feature points has a flexible direction instead of a fixed one. According to the image intensities at the interest pixel location, the direction of the window is based on the largest gradient direction. Similarly, the DIC process can use a subset that is not only self-adaptive in size but also in orientation; such a self-adaptive shape can help yield a better correlation result. It is noted that some DIC researchers have recently adopted ideas from the IRM techniques in computer vision to use Gaussian weight window to put more weight in the interrogated pixel and its closer neighbors than the further away pixels in the subset [66,67].

Compared with the IRM technique, the DIC technique puts a stronger emphasis on accuracy because it is critical in experimental mechanics applications. To obtain high accuracy, the DIC technique has to sacrifice its analysis speed, and this becomes a subject that researchers have attempted to improve [13,68]. With more advanced algorithms and schemes (such as reliability-guided scanning strategy and self-adaptive subset) incorporated into the DIC technique, the processing speed can be substantially affected. To enhance the processing speed, GPU-based parallel computation such as compute unified device architecture (CUDA) platform can be exploited. A feasible way is to use SURF and FAST algorithms to detect a certain number of seed points for the DIC analysis, and the subsequent DIC analysis is carried out on each point and its reliability-guided neighbors [44] in a parallel mode.

Other notable measures used by the IRM techniques that can be suitable for DIC applications include employing integral images to enhance processing speed, enforcing local disparity consistency to prevent large errors, and applying image segmentation and local-global cost aggregation to cope with the boundary issues associated with multiple separate regions.

Fig. 9 demonstrates an application of the DIC technique to the 3D surface profile measurement of a curved sample of road pavement, where the sample surface has natural microtexture patterns available for the image correlation and matching task. The SIFT algorithm and the self-adaptive subset scheme were utilized in the DIC analysis.

5. Discussion and conclusion

The DIC and IRM techniques have become one of the most, if not the most, widely used techniques in the fields of experimental mechanics and computer vision, respectively. Although the two techniques are very similar and both involve detecting the same physical points in two or more images, the experimental mechanics and computer vision communities nearly have no dialog between them in the past. As technologies evolve, more and more communications between the two communities are necessary. In this paper, comparison of the DIC and IRM techniques is reviewed, and their similarities and differences are identified. On one hand, it is shown that both techniques use the area-based scheme for reliable image matching, and both rely on advanced camera calibration for accurate applications. On the other hand, the DIC and IRM techniques have a number of differences: the DIC technique usually uses artificial speckle patterns and area-based matching to obtain high-accuracy analysis with relatively low speed for controlled measurements, whereas the IRM technique often uses natural texture patterns with

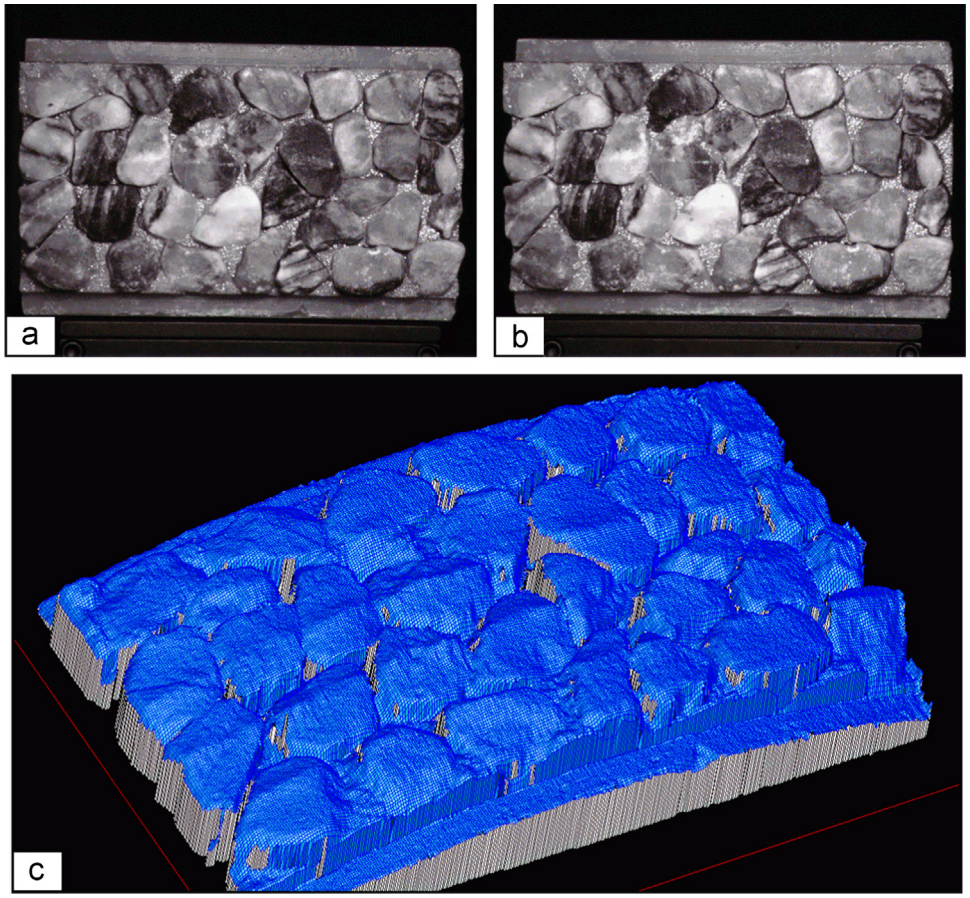

Fig. 9. 3D surface profile measurement of a polished coarse aggregate sample of road pavement. (a), (b) Images captured by two cameras and (c) the 3D plot.

both area- and feature-based matching to reach fast processing with relatively low accuracy for general applications.

The similarities and differences as well as advantages and disadvantages of the DIC and IRM techniques make the complements between them feasible. In this paper, emphasis is put on incorporating some concepts from the IRM technique into the DIC technique to achieve enhanced performance, such as adopting natural texture patterns to improve efficiency and simplify measurements, using feature-based matching to carry out automated initial guess in the case of large deformation and/or rotation and perform automated DIC analysis for multiple separate scenes and/or objects encountered in practical applications, utilizing self-adaptive subset to enhance analysis accuracy and processing speed, and employing GPU-based parallel computing to speed up the advanced DIC analysis.

This paper does not aim to give a comprehensive and thorough review on the DIC and IRM techniques. Instead, it targets to introduce the advanced algorithms from the computer vision field to the experimental mechanics as well as the optical measurement fields. The goal is to help broaden the applications of the DIC technique, which is capable of accurately performing 2D/3D deformation and shape measurements with great ease, in ever-increasing scientific research and engineering practice.

Acknowledgments

This work was partially supported by the United States Army Research Office under grant W911NF-10-1-0502. Z. Wang is grateful to Minh Vo at Carnegie Mellon University for helpful discussions.

References

[1] McGlone J, Mikhail E, Bethel J. Manual of photogrammetry. Bethesda, Maryland, USA: ASPRS; 2013.
[2] Peters W, Ranson W. Digital imaging techniques in experimental stress analysis. Opt Eng 1982;21(3):427–31.
[3] Sutton M, Wolters W, Peters W, Ranson W, McNeill S. Determination of displacements using an improved digital correlation method. Image Vis Comput 1983;1(3):133–9.
[4] Peters W, Ranson W, Sutton M, Chu T, Anderson J. Application of digital correlation methods to rigid body mechanics. Opt Eng 1983;22(6):738–42.
[5] Chu T, Ranson W, Sutton M, Peters W. Applications of digital image correlation techniques to experimental mechanics. Exp Mech 1985;25(3):232–44.
[6] Sutton M, Cheng M, Peters W, Chao Y, McNeill S. Application of an optimized digital correlation method to planar deformation analysis. Image Vis Comput 1986;4(3):143–50.
[7] Bruck H, McNeill S, Sutton M, Peters W. Digital image correlation using Newton–Raphson method of partial differential correction. Exp Mech 1989;29(3):261–7.
[8] Pan B, Qian K, Xie H, Asundi A. Two-dimensional digital image correlation for in-plane displacement and strain measurement: a review. Meas Sci Technol 2009;20:062001.
[9] Sutton M, Orteu J, Schreier H. Image correlation for shape, motion, and deformation measurements. New York, USA: Springer; 2009.
[10] Brown L. A survey of image registration techniques. ACM Comput Surv 1992;24(4):325–76.
[11] Lucas B, Kanade T. An iterative image registration technique with an application to stereo vision. In: Proceedings of the international joint conference on artificial intelligence; August 1981. p. 674–9.
[12] Baker S, Matthews I. Lucas–Kanade 20 years on: a unifying framework. Int J Comput Vis 2004;56(3):221–55.
[13] Pan B, Li K, Tong W. Fast, robust and accurate digital image correlation calculation without redundant computations. Exp Mech 2013;53(7):1277–89.
[14] Scharstein D, Szeliski R. A taxonomy and evaluation of dense two-frame stereo correspondence algorithms. Int J Comput Vis 2002;47(1/2/3):7–42.
[15] ⟨http://vision.middlebury.edu/stereo/⟩.
[16] Pan B, Xie H, Wang Z. Equivalence of digital image correlation criteria for pattern matching. Appl Opt 2010;49(28):5501–9.
[17] Luu L, Wang Z, Vo M, Hoang T, Ma J. Accuracy enhancement of digital image correlation with B-spline interpolation. Opt Lett 2011;36(16):3070–2.

[18] Wang M, Wang H, Cen Y. High-speed digital image correlation method. Opt Lett 2009;34(13):1955–7.
[19] Wang Z, Hoang T, Nguyen D, Urcinas A, Magro J. High-speed digital image correlation method: comment. Opt Lett 2010;35(17):2891.
[20] Tsai R. A versatile camera calibration technique for high accuracy 3D machine vision metrology using off-the-shelf TV cameras and lenses. IEEE J Robot Autom 1987;3(4):323–44.
[21] Zhang Z. A flexible new technique for camera calibration. IEEE Trans Pattern Anal Mach Intell 2000;22(11):1330–4.
[22] Heikkila J. Geometric camera calibration using circular control points. IEEE Trans Pattern Anal Mach Intell 2000;22(10):1066–77.
[23] Song L, Wang M, Lu L, Huan H. High precision camera calibration in vision measurement. Opt Lasers Technol 2007;39(7):1413–20.
[24] Wang J, Shi F, Zhang J, Liu Y. A new calibration model of camera lens distortion. Pattern Recognit 2008;41(2):607–15.
[25] Mirzaei F, Roumeliotis S. A Kalman filter-based algorithm for IMU-camera calibration: observability analysis and performance evaluation. IEEE Trans Robot 2008;24(5):1143–56.
[26] Strecha C, von Hansen W, Van Gool L, Fua P, Thoennessen U. On benchmarking camera calibration and multi-view stereo for high resolution imagery. IEEE Conf Comput Vis Pattern Recognit 2008:1–8.
[27] Furukawa Y, Ponce J. Accurate camera calibration from multi-view stereo and bundle adjustment. Int J Comput Vis 2009;84(3):257–68.
[28] Douxchamps D, Chihara K. High-accuracy and robust localization of large control markers for geometric camera calibration. IEEE Trans Pattern Anal Mach Intell 2009;31(2):376–83.
[29] Hartley R, Zisserman A. Multiple view geometry in computer vision. 2nd ed.. Cambridge, UK: Cambridge University Press; 2004.
[30] Vo M, Wang Z, Luu L, Ma J. Advanced geometric camera calibration for machine vision. Opt Eng 2011;50(11):110503.
[31] Vo M, Wang Z, Pan B, Pan T. Hyper-accurate flexible calibration technique for fringe-projection-based three-dimensional imaging. Opt Express 2012;20 (15):16926–41.
[32] Zitova B, Flusser J. Image registration methods: a survey. Image Vis Comput 2003;21(11):977–1000.
[33] Lecompte D, Smits A, Bossuyt S, Sol H, Vantomme J, Van Hemelrijck D, et al. Quality assessment of speckle patterns for digital image correlation. Opt Lasers Eng 2006;44(11):1132–45.
[34] Lowe D. Distinctive image features from scale-invariant keypoints. Int J Comput Vis 2004;60(2):91–110.
[35] Bay H, Ess A, Tuytelaars T, Van Gool L. Speeded-up robust features (SURF). Comput Vis Image Underst 2008;110(3):346–59.
[36] Ke Y, Sukthankar R. PCA-SIFT: a more distinctive representation for local image descriptors. IEEE Comput Soc Conf Comput Vis Pattern Recognit 2004;2:506–13.
[37] Muja M, Lowe D. Fast matching of binary features. In: Conference on computer and robot vision; 2012. p. 404–10.
[38] Fischler M, Bolles R. Random sample consensus: a paradigm for model fitting with applications to image analysis and automated cartography. Commun ACM 1981;24(6):381–95.
[39] Chum O, Matas J. Matching with PROSAC—progressive sample consensus. In: IEEE computer society conference on computer vision and pattern recognition; 2005. p. 220–6.
[40] Ni K, Jin H, Dellaert F. GroupSAC: efficient consensus in the presence of groupings. In: IEEE 12th international conference on computer vision; 2009. p. 2193–200.
[41] Wang Z, Vo M, Kieu H, Pan T. Automated fast initial guess in digital image correlation. Strain 2014;50(1):28–36.
[42] Smith S, Brady J. SUSAN—a new approach to low level image processing. Int J Comput Vis 1997;23(1):45–78.
[43] Rosten E, Drummond T. Machine learning for high-speed corner detection. In: Proceedings of the 9th European conference on computer vision, vol. 3951; 2006. p. 430–43.
[44] Pan B, Wang Z, Lu Z. Genuine full-field deformation measurement of an object with complex shape using reliability-guided digital image correlation. Opt Express 2010;18(2):1011–23.
[45] Mei X, Sun X, Zhou M, Jiao S, Wang H, Zhang X. On building an accurate stereo matching system on graphics hardware. IEEE Int Conf Comput Vis Workshops 2011;1:467–74.
[46] Klaus A, Sormann M, Karner K. Segment-based stereo matching using belief propagation and a self-adapting dissimilarity measure. In: 18th international conference on pattern recognition, vol. 3; 2006. p. 15–8.
[47] Wang Z, Zheng Z. A region based stereo matching algorithm using cooperative optimization. In: IEEE conference on computer vision and pattern recognition; 2008. p. 1–8.
[48] Sun X, Mei X, Jiao S, Zhou M, Wang H. Stereo matching with reliable disparity propagation. In: International conference on 3D imaging, modeling, processing, visualization and transmission; 2011. p. 132–9.
[49] Yang Q, Wang L, Yang R, Stewenius H, Nister D. Stereo matching with color-weighted correlation, hierarchical belief propagation and occlusion handling. IEEE Trans Pattern Anal Mach Intell 2009;31(3):492–504.
[50] Cofaru C, Philips W, VanPaepegem W. Pixel-level robust digital image correlation. Opt Express 2013;21(24):29979–99.
[51] Zhang D, Luo M, Arola D. Displacement/strain measurements using an optical microscope and digital image correlation. Opt Eng 2006;45(3):033605.
[52] Sjogren T, Persson P, Vomacka P. Analysing the deformation behaviour of compacted graphite cast irons using digital image correlation techniques. Key Eng Mater 2010;457:470–5.
[53] Zhou Z, Chen P, Huang F, Liu S. Experimental study on the micromechanical behavior of a PBX simulant using SEM and digital image correlation method. Opt Lasers Eng 2011;49(3):366–70.
[54] Baldit A, Ambard D, Cherblanc F, Royer P. Digital image correlation on annulus fibrosus soft tissue. In: Proceedings of photomechanics conference; 2013.
[55] Marcellier H, Vescovo P, Varchon D, Vacher P, Humbert P. Optical analysis of displacement and strain fields on human skin. Skin Res Technol 2001;7 (4):246–53.
[56] Kieu H, Pan T, Wang Z, Le M, Nguyen H, Vo M. Accurate 3D shape measurement of multiple separate objects with stereo vision. Meas Sci Technol 2014;25(3):035401.
[57] Zhou Y, Chen Y. Feature matching for automated and reliable initialization in three-dimensional digital image correlation. Opt Lasers Eng 2013;51 (3):213–23.
[58] Haddadi H, Belhabib S. Use of rigid-body motion for the investigation and estimation of the measurement errors related to digital image correlation technique. Opt Lasers Eng 2008;46(2):185–96.
[59] Sun Y, Pang H. Study of optimal subset size in digital image correlation of speckle pattern images. Opt Lasers Eng 2007;45(9):967–74.
[60] Pan B, Xie H, Wang Z, Qian K, Wang Z. Study on subset size selection in digital image correlation for speckle patterns. Opt Express 2008;16(10):7037–48.
[61] Fazzini M, Mistou S, Dalverny O, Robert L. Study of image characteristics on digital image correlation error assessment. Opt Lasers Eng 2010;48(3):335–9.
[62] Ning J, Braxton V, Wang Y, Sutton M, Wang Y, Lessner S. Speckle patterning of soft tissues for strain field measurement using digital image correlation: preliminary quality assessment of patterns. Microsc Microanal 2011;17 (1):81–90.
[63] Pan B. Bias error reduction of digital image correlation using Gaussian pre-filtering. Opt Lasers Eng 2013;51(10):1161–7.
[64] Crammond G, Boyd S, Dulieu-Barton J. Speckle pattern quality assessment for digital image correlation. Opt Lasers Eng 2013;51(12):1368–78.
[65] Zappa E, Mazzoleni P, Matinmanesh A. Uncertainty assessment of digital image correlation method in dynamic applications. Opt Lasers Eng 2014;56:140–51.
[66] Huang J, Pan X, Peng X, Yuan Y, Xiong C, Fang J, et al. Digital image correlation with self-adaptive Gaussian windows. Exp Mech 2013;53(3):505–12.
[67] Yuan Y, Huang J, Peng X, Xiong C, Fang J, Yuan F. Accurate displacement measurement via a self-adaptive digital image correlation method based on a weighted ZNSSD criterion. Opt Lasers Eng 2014;52:75–85.
[68] Pan B, Li K. A fast digital image correlation method for deformation measurement. Opt Lasers Eng 2011;49(7):841–7.